Supplementary Materials: L-Band Polarimetric Target Decomposition of Mangroves of the Rufiji Delta, Tanzania. *Remote Sensing* 2016, *8*, 140.

Ian Brown, Simon Mwansasu and Lars-Ove Westerberg

Table S1 describes the target decomposition results for the field study sites (Figure 1). All sites exhibit high entropy (>0.7). Anisotropy is generally in the 0.2–0.4 range, with a notable exception being Site 14A, which is situated in a stand of relatively small *Rhizophora mucronata.* This stand occupies mudbanks and creek margins. Mean alpha angles are low here. Site 16A, which also includes inundated mangroves (*Sonneratia alba*) has high double-bounce scattering according to the Yamaguchi decomposition and has high values from the Cloude decomposition second term. Site 8A, a cultivated island with coconut trees and palms, is the most similar to Site 16A. Table 1 is included to complement Figures 3 and 4.

Table S1. Target decomposition values for the selected test (see Figure 1). The Yamaguchi decomposition is abbreviated to G4U (an abbreviation of general four-component decomposition with unitary transformation).

Site	Decomposition Year	Entropy H	Anisotropy A	Alpha $\bar{\alpha}$	G4U Double-Bounce (dB)	G4U Volume (dB)	G4U Surface (dB)
3A Rice fields with mangrove remnants	2007	0.85	0.40	47	−9.5	−7.2	−10.0
	2009	0.86	0.30	47	−10.0	−6.4	−10.5
	2010	0.84	0.18	43	−14.0	−8.0	−11.0
5A *Avicennia* dominant	2007	0.83	0.32	46	−11.0	−8.2	−11.0
	2009	0.82	0.30	46	−11.0	−7.7	−10.5
	2010	0.83	0.35	44	−13.0	−10	−11.5
8A Island settlement, rice fields/coconut trees	2007	0.83	0.47	50	−8.0	−8.0	−9.6
	2009	0.75	0.43	51	−7.7	−10.0	−11.5
	2010	0.77	0.23	33	−20.0	−9.6	−11.0
9A Almost pure *Avicennia*	2007	0.83	0.32	46	−11.5	−8.0	−11.5
	2009	0.84	0.29	47	−11.5	−8.5	−12.2
	2010	0.83	0.33	45	−14.0	−9.6	−11.5
11A *Sonneratia*, evidence of harvesting	2007	0.76	0.30	48	−8.5	−8.0	−11.6
	2009	0.75	0.32	46	−8.9	−7.7	−9.6
	2010	0.76	0.36	44	−10.5	−9.2	−10.0
14A *Small Rhizophora*, many small creeks	2007	0.84	0.13	39	−15.2	−5.8	−9.2
	2009	0.81	0.14	37	−15.2	−5.2	−7.5
	2010	0.83	0.17	39	−15.2	−5.7	−8.5
16A *Sonneratia*, in sea water	2007	0.78	0.30	51	−7.7	−7.7	−13.0
	2009	0.74	0.27	52	−6.8	−8.9	−12.2
	2010	0.74	0.31	50	−6.8	−8.2	−11.5

The $H/A/\bar{\alpha}$ data for 2007 and 2010 are presented in Figure S1 to complement the data presented in Figure 1 (in the main text). The high entropy over the mangrove forest in the 2007 data is evident as are the low $\bar{\alpha}$ values over the grasslands in the 2010 data. The 2010 data also exhibit regions of slightly higher anisotropy, relative to the other image data, in the northern delta mangroves. This is confirmed in Table S1. (Sites 5A, 9A, 11A, 14A). Low anisotropy may indicate a single dominant scattering mechanism or a random type of scattering [24].

Wishart classifiers applied to the $H/\bar{\alpha}$ and Yamaguchi target decompositions from 2007 are shown in Figure S2. The colour assignment is random. The $H/\bar{\alpha}$ classification appears to have resulted in generalized scattering mechanism classes: two surface scattering classes in yellow and cyan and two volume scattering-dominated classes in red and green. The Yamaguchi Wishart classification appears more nuanced with a spectrum of yellow-orange-red classes assigned to mangroves and blue-cyan assigned to surface scattering. Double-bounce-dominated regions are in green. The level of detail in the mangrove forest is greatest in the Yamaguchi results.

The entropy-alpha plane region corresponding to these $H/\bar{\boldsymbol{\alpha}}$ values is classified as anisotropic particles, resulting in volume diffusion (Figure S3) [24, 34]. This would be a logical description of scattering from dense mangrove canopy. The Wishart $H/\bar{\boldsymbol{\alpha}}$ classifier (Figure S2) produces nine classes, including "unclassified". The differences in class composition between years emphasizes the role of tidal and fluvial inundation on the polarimetric response of mangroves and rice paddies. Moisture content has previously been found to affect forest classification using Wishart $H/\bar{\boldsymbol{\alpha}}$ classifiers [36, 37]. $H/A/\bar{\boldsymbol{\alpha}}$ Wishart classifications resulted in a similar pattern to the H/$\bar{\boldsymbol{\alpha}}$ Wishart classifier. Of the available 16 classes, six or seven contained no data. The 2010 classification included three classes, corresponding to surface scattering, and all datasets produced four forest/mangrove classes. However, differences in mangrove classes are evident between the datasets. The 2007 and 2009 results include a class that maps mangrove stands along creeks and on the margins of raised lands; this class does not appear in the 2010 classification. Nevertheless, the Wishart results from the $H/\bar{\boldsymbol{\alpha}}$ and $H/A/\bar{\boldsymbol{\alpha}}$ decompostions were of limited value, only providing generalized classes. $H/\bar{\boldsymbol{\alpha}}$ classification has proven problematic in tropical forest sites [36]. High values of H led to drastic reduction of the classification accuracy compared to stands with $H \leq 0.6$ [36]. The Wishart classifier applied to the volume, surface and double-bounce scattering terms resulting from the Yamaguchi target decomposition did not produce empty classes lacking data. The greater complexity provided a more nuanced image of the land cover of the delta and of the organization of the mangrove forests (Figure S2). In Amazonian forest, riparian sites could be differentiated from primary forest by slightly lower entropy (≤0.85) pastures, some of which retained selected trees species, exhibiting a wide range of entropy and alpha values [37].

The $H/\bar{\alpha}$ planes for each of the three PALSAR datasets are shown in Figure S3. The datasets from 2007 and 2009 are similar, while the pattern projected in the $H/\bar{\alpha}$ plane by the 2010 data differs substantially. The latter lacks distinct dihedral reflector targets and has greater presence in the Bragg scattering region. This is evident in the 2010 data, where the grasslands exhibit low scattering and a dominant surface scattering mechanism. Figure S3 may be useful as an aid to the discussion of $H/A/\bar{\alpha}$ decomposition patterns and supports the analysis of Figure 3 in the main text.

Figures S4, S5 and S6 show the results of the entropy and Arii decompositions. These figures aim to add detail to the descriptions in the text and are meant to provide additional reference in support of the Results and Discussion sections. Figures S4 and S6 show detail

from the Arii double-bounce (red), volume (green) and surface scattering (blue) components. These can be compared to the entropy results in Figure S5.

Figure S7 provides readers with examples of the PRISM and IKONOS data that we used in support of our analyses. The very high resolution of these data allows us to qualitatively analyze the density of forest, relative stand heights and identify inundation where it occurs. Evidence of human activity, such as farming and felling, was also derived from these data.

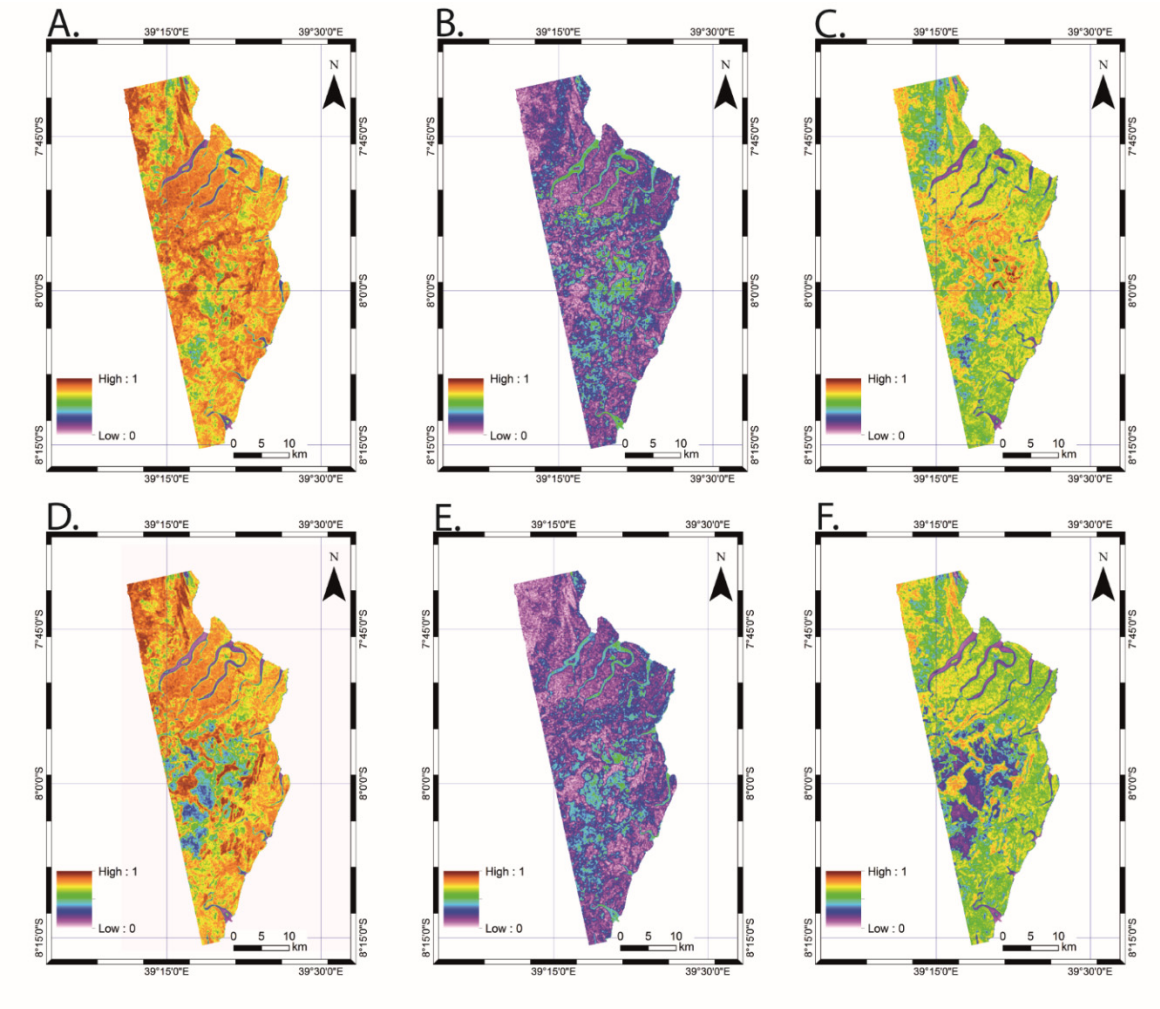

Figure S1. H/A/$\bar{\alpha}$ decompositions for 2007 ((**A**–**C**), respectively) and 2010 (**D**–**F**). Note the low anisotropy over much of the mangrove forests. High alpha angles are found over non-forest sites and where agriculture has not been developed.

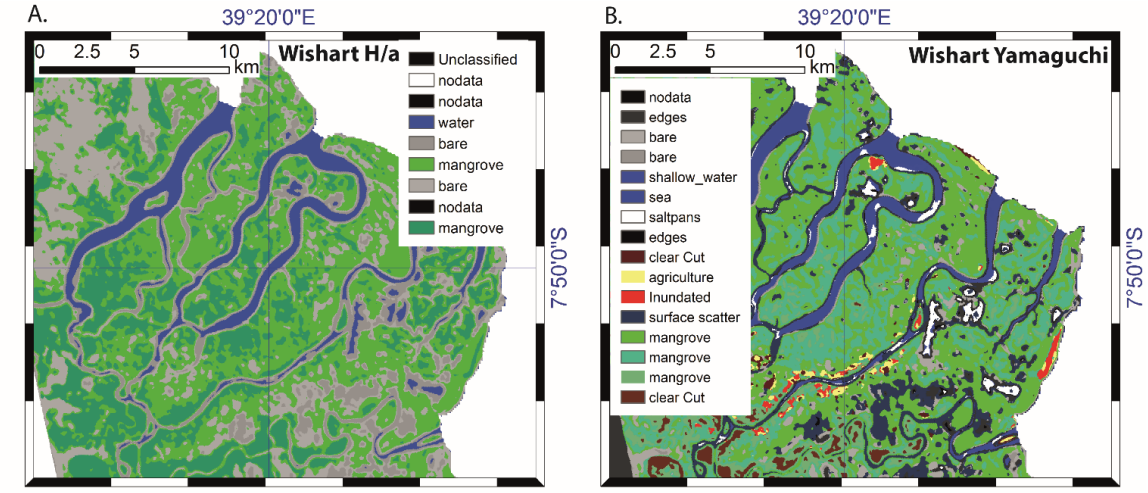

Figure S2. Comparison of Wishart classifiers using data from 2007. The assignment of class orders is arbitrary; class colors are ordered blue-green-red (starting with Class 1). (A) Wishart H/$\bar{\alpha}$ classification using nine classes, five of which lacked data. (B) Wishart classifier applied to the volume, double-bounce and surface scattering terms of the Yamaguchi decomposition. Sixteen classes were mapped using all of the available classification space (including unclassified). The Yamaguchi scattering model classification resulted in greater complexity and considerably less generalization.

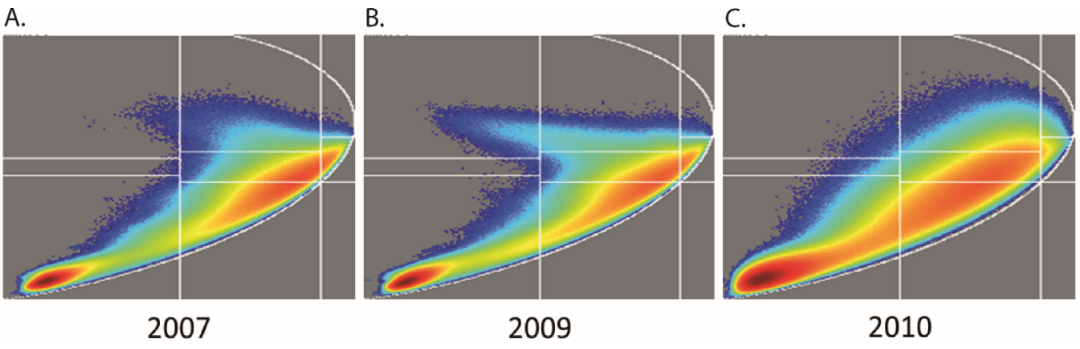

Figure S3. The H/$\bar{\alpha}$ plane showing the density distribution of the target responses. The pattern for 2010 data differs greatly from the other two datasets. 2010 exhibits a greater concentration around the surface scattering and anisotropic particle zones with less of a tail extending into the dihedral reflector zone. 2009 displays the greatest distribution of dihedral reflectors.

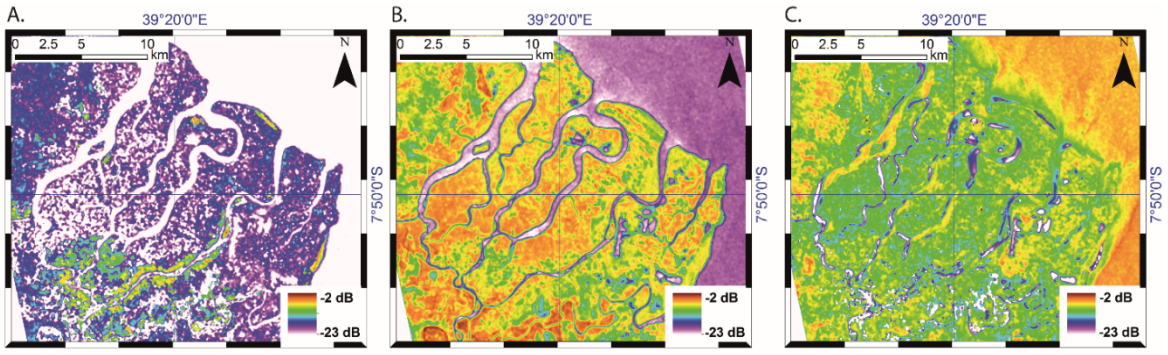

Figure S4. Arii decomposition elements from PALSAR data from 2007 over the northern Rufiji Delta, Tanzania. (A) Double-bounce scattering is low throughout the mangrove area. The highest double-bounce occurs in association with agriculture and cleared forest along the rivers in the west. (B) Volume scattering is high throughout the mangrove forest. Lower volume scattering (green) is found over grasslands and scrub vegetation. (C) Surface scattering: highest where forest has been

cleared and in the Rhizophora populated region in the northeast of the delta, where canopy closure is low.

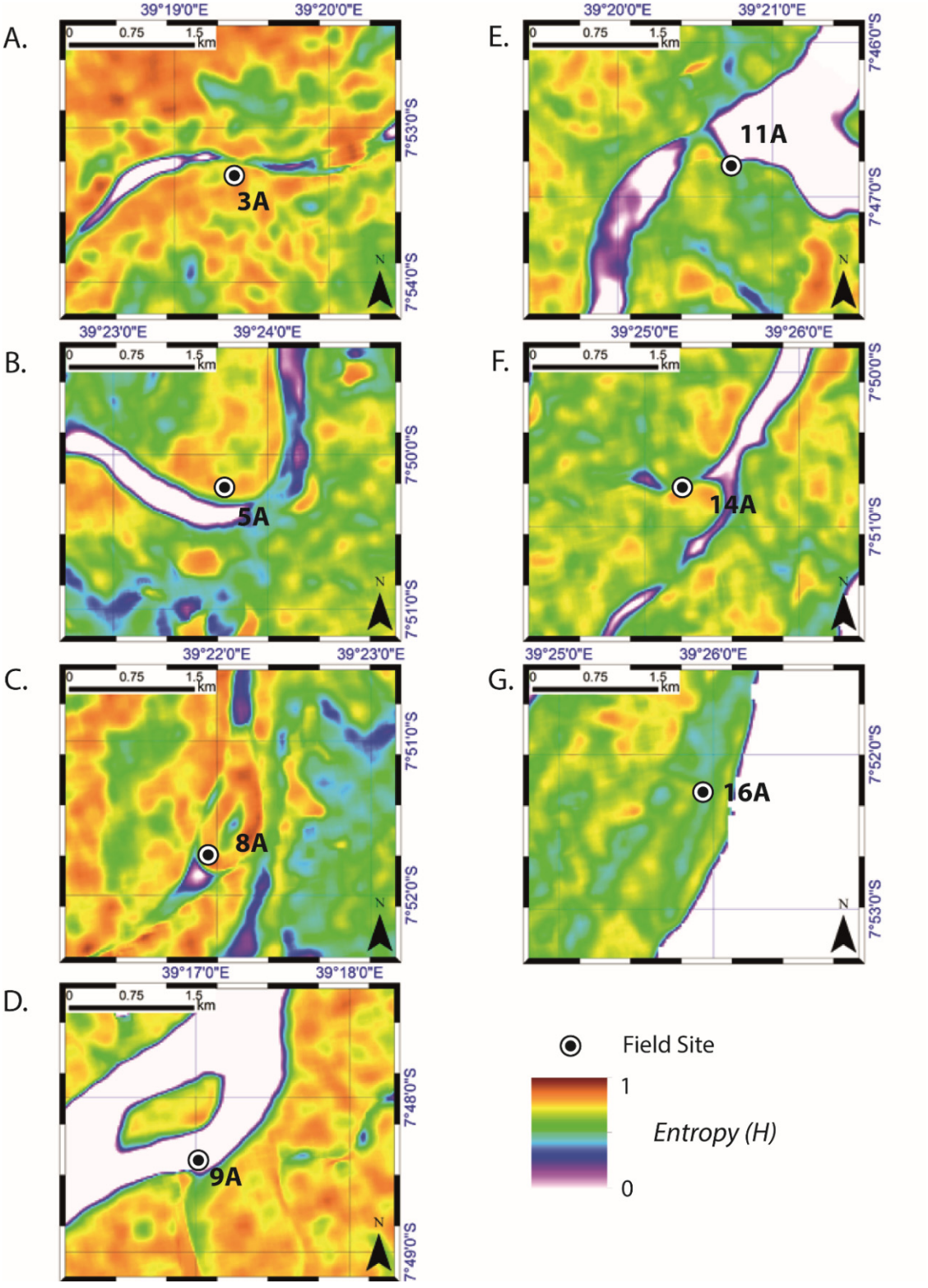

Figure S5. Detail of entropy decompositions for the study sites. Note the greater averaging in the entropy data (relative to the model decomposition in Figure S6, below).

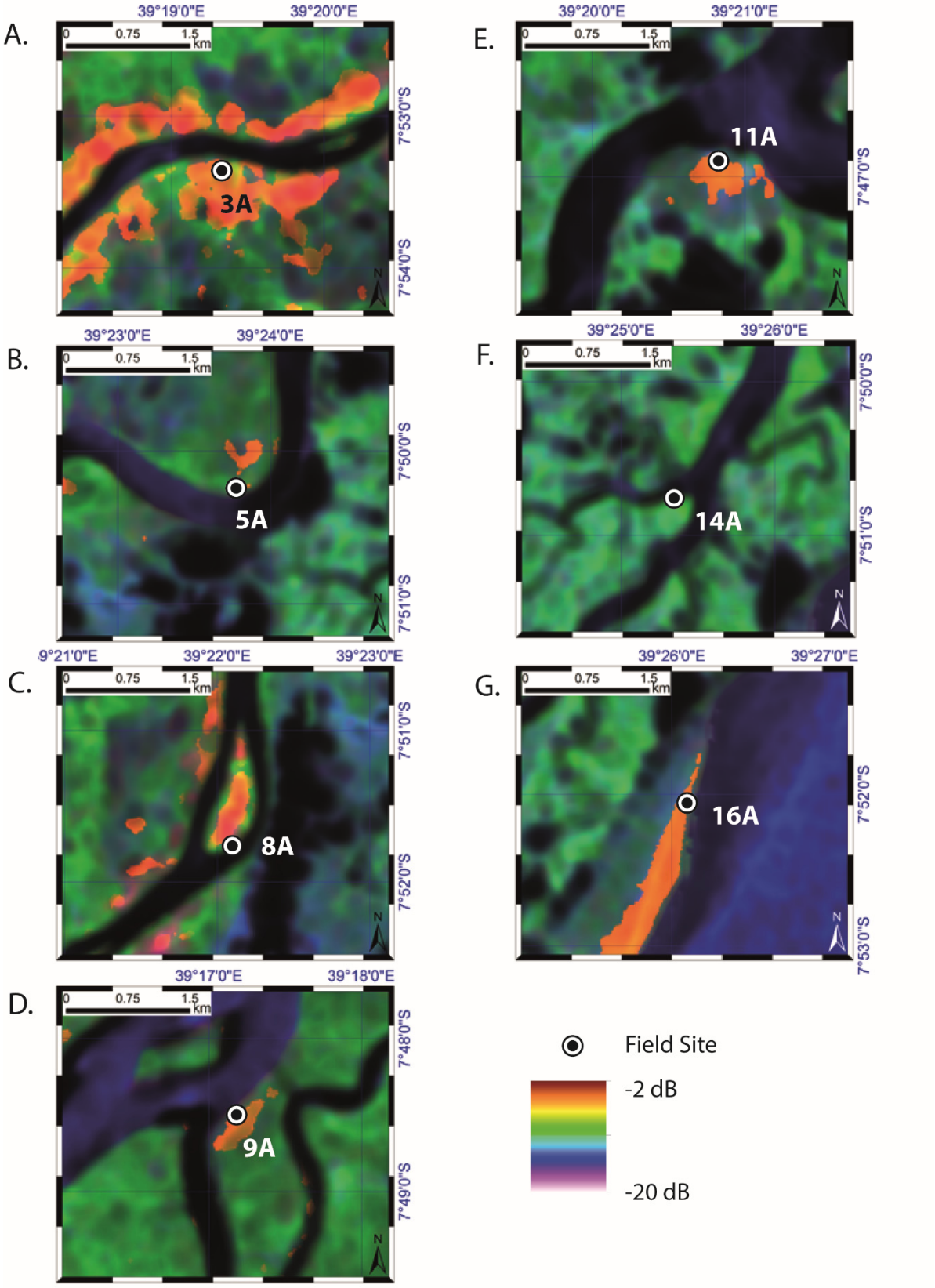

Figure S6. False color composites of the Arii decomposition from 2007 over the study sites. Double-bounce scattering is shown in red, volume scattering in green and surface scattering in blue.

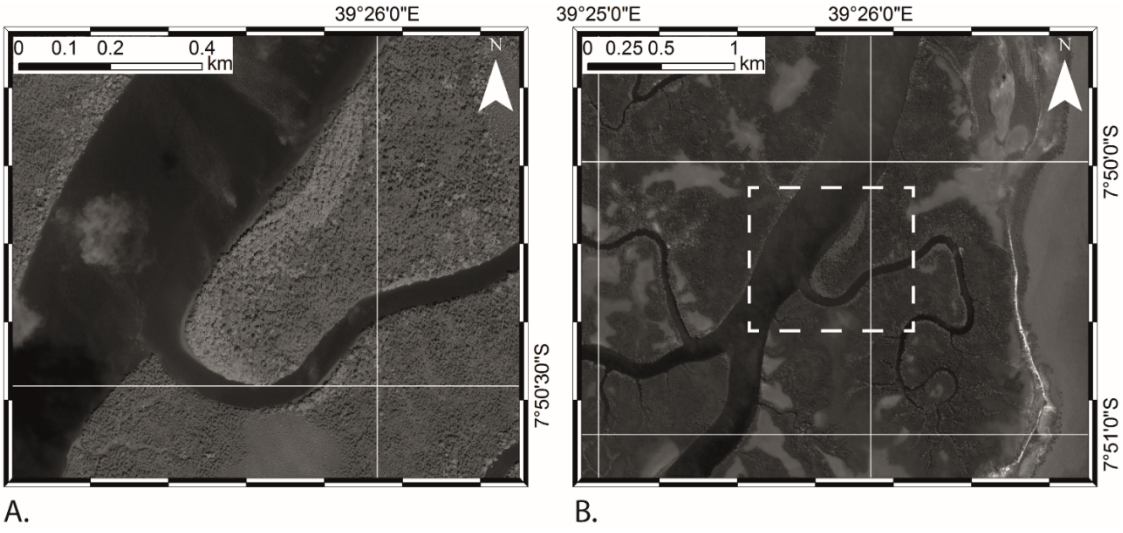

Figure S7. Image subsets showing the native resolution of the optical data used in support of the SAR data analysis. (**A**) IKONOS-2 image subset at full resolution. (**B**) ALOS PRISM image over the same region with the IKONOS-2 full resolution subset area shown as a white dashed box. Note the local differences in mangrove species evident as grayscale reflectance differences.